Acta Oceanol. Sin., 2022, Vol. 41, No. 7, P. 84–96
https://doi.org/10.1007/s13131-021-1967-z
http://www.aosocean.com
E-mail: ocean2@hyxb.org.cn

Characteristics and influencing factors of frontal upwelling in the Yellow Sea in summer

Fan Sun[1, 2, 3, 4], Fei Yu[1, 3, 4, 5, 6*], Guangcheng Si[1, 3, 4], Jianfeng Wang[1, 3, 4], Anqi Xu[1, 3, 4], Jun Pan[1, 3, 4, 7], Ying Tang[1, 3, 4]

[1] Institute of Oceanology, Chinese Academy of Sciences, Qingdao 266071, China

[2] Tianjin Navigation Instruments Research Institute, Tianjin 300131, China

[3] University of Chinese Academy of Sciences, Beijing 100049, China

[4] Key Laboratory of Ocean Circulation and Waves, Chinese Academy of Sciences, Qingdao 266071, China

[5] Center for Ocean Mega-Science, Chinese Academy of Sciences, Qingdao 266071, China

[6] Laboratory for Ocean Dynamics and Climate, Pilot National Laboratory for Marine Science and Technology (Qingdao), Qingdao 266237, China

[7] Center for Marine Environmental Engineering, Institute of Oceanology, Chinese Academy of Sciences, Qingdao 266071, China

Received 13 April 2021; accepted 30 September 2021

Abstract

Frontal upwelling is an important phenomenon in summer in the Yellow Sea (YS) and plays an essential role in the distribution of nutrients and biological species. In this paper, a three-dimensional hydrodynamic model is applied to investigate the characteristics and influencing factors of frontal upwelling in the YS. The results show that the strength and distribution of frontal upwelling are largely dependent on the topography and bottom temperature fronts. The frontal upwelling in the YS is stronger and narrower near the eastern coast than near the western coast due to the steeper shelf slope. Moreover, external forcings, such as the meridional wind speed and air temperature in summer and the air temperature in the preceding winter and spring, have certain influences on the strength of frontal upwelling. An increase in air temperature in the previous winter and spring weakens the frontal upwelling in summer; in contrast, an increase in air temperature in summer strengthens the frontal upwelling. When the southerly wind in summer increases, the upwelling intensifies in the western YS and weakens in the eastern YS. The air temperature influences the strength of upwelling by changing the baroclinicity in the frontal region. Furthermore, the meridional wind speed in summer affects frontal upwelling via Ekman pumping.

Key words: influencing factors, Yellow Sea, frontal upwelling, bottom temperature fronts, numerical study

Citation: Sun Fan, Yu Fei, Si Guangcheng, Wang Jianfeng, Xu Anqi, Pan Jun, Tang Ying. 2022. Characteristics and influencing factors of frontal upwelling in the Yellow Sea in summer. Acta Oceanologica Sinica, 41(7): 84–96, doi: 10.1007/s13131-021-1967-z

1 Introduction

The Yellow Sea (YS) is a shallow, semienclosed basin located in the Northwest Pacific Ocean and is surrounded by the Korean Peninsula and the Chinese mainland (Fig. 1a). It has an average depth of 44 m and a maximum depth of less than 100 m. Due to the limited depth and geological conditions, the hydrographic properties of the YS are strongly affected by the monsoon system.

In winter, a strong northwesterly wind prevails in the YS, with the effects of surface cooling and wind stirring, and the entire water column in the YS mixes homogenously. During this time, the sea is ventilated, and atmospheric signals can be transmitted throughout the water column. From spring to summer, the surface water begins to warm in association with the increase in solar radiation, and a thermocline begins to form, which isolates the relatively cold water below the thermocline and forms the Yellow Sea Cold Water Mass (YSCWM) (He et al., 1959; Mao et al., 1964; Zhang et al., 1983; Hur et al., 1999; Ren and Zhan, 2005; Yu et al., 2006).

Along the boundary of the YSCWM, the tidal mixing front separates the cold, stratified water on the offshore side from the warm, well-mixed water on the other side (Lü et al., 2010). The formation of the tidal mixing front is closely related to the turbulent kinetic energy induced by the tidal current under the effect of bottom friction (Simpson and Hunter, 1974; Zhao, 1986). The turbulent stress works against the buoyancy force and produces tidal mixing fronts at the bottom. The tidal mixing front has a great impact on the three-dimensional circulation in summer. On the one hand, the tidal mixing front generates a basin-scale cyclonic circulation in the upper layer of the YS, which is known as the Yellow Sea Cold Water Mass circulation (YSCWMC) and

Foundation item: The National Key Research and Development Project under contract No. 2017YFC1403400; the National Key Research and Development Program of China under contract No. 2016YFC1402501; the National Natural Science Foundation of China under contract No. 41806164; the Open Fund Project of Key Laboratory of Marine Environmental Information Technology, Ministry of Natural Resources; the Shandong Joint Fund for Marine Science Research Centers under contract No. U1406401.
*Corresponding author, E-mail: yuf@qdio.ac.cn

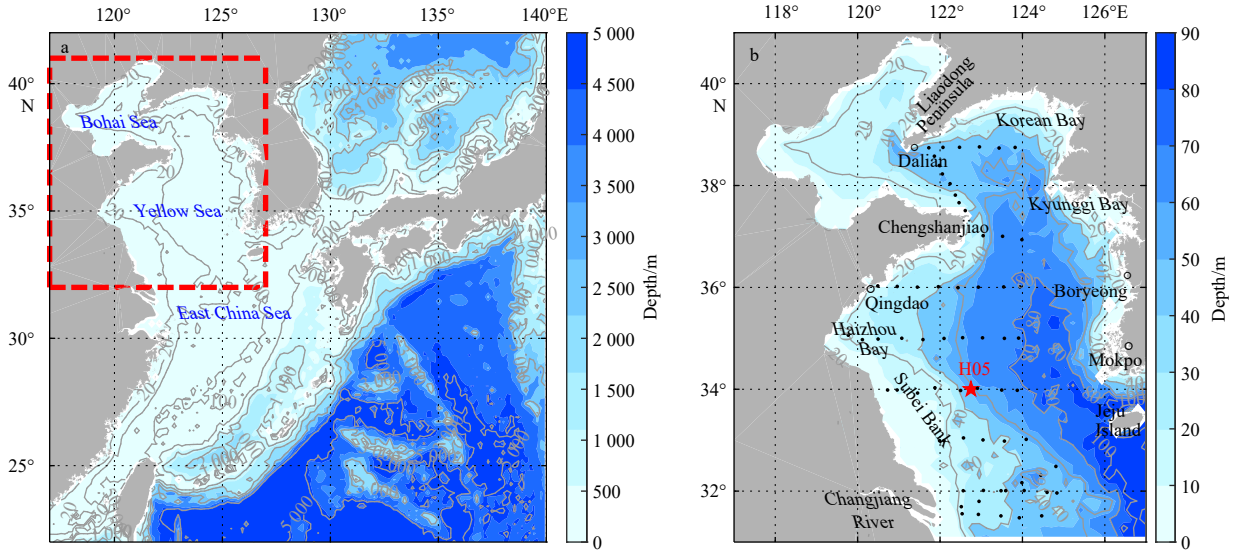

Fig. 1. Model domain with topography (a), and map of the study area (b). The red dashed box represents the location of the Yellow Sea and Bohai Sea. Coloured shading and grey solid lines denote bathymetry (in m). The black dots represent the locations of conductivity-temperature-depth profiler stations from the cruise surveys in August 2015. The red star represents the H05 mooring station.

has been reported in many observational and numerical studies (Beardsley et al., 1992; Feng et al., 1992; Yanagi and Takahashi, 1993; Naimie et al., 2001; Xu et al., 2003; Xia et al., 2006; Zhou et al., 2015; Lie and Cho, 2016). On the other hand, it triggers frontal upwelling over the slope in the YS (Lü et al., 2010).

Frontal upwelling is an important phenomenon in summer in the YS and exerts a great influence on the distributions of nutrients and biological species. The upwelling carries nutrients (phosphates, nitrates, etc.) from the bottom layer to the upper layer of the YS, which is favourable to the growth and reproduction of phytoplankton. Furthermore, frontal upwelling has a significant effect on the hydrographic features of the YS. In summer, surface cold patches (SCPs) are often observed along the boundary of the YSCWM, especially offshore of the Shandong, Liaodong and Korean peninsulas (Garrett and Loucks, 1976; Xia and Guo, 1983; Lie, 1986; Zou et al., 2001). Xia and Guo (1983) suggested that the sustained SCPs offshore of the Shandong and Liaodong peninsulas are most likely caused by strong upwelling. Thereafter, a numerical model based on thermodynamic equations was applied to describe the upwelling in the YS (Guo and Xia, 1986), and the results indicated that upwellings off Chengshanjiao and the Liaodong Peninsula are mainly induced by centrifugal forces related to the strong tidal current flowing headlands.

Based on satellite images and hydrological investigations, Zhao (1987a, b) found that upwelling mainly exists in the frontal area in the western YS and inferred that upwelling is possibly widespread along the boundary of the YSCWM. Subsequently, the vertical upwelling structure near the frontal area was investigated by a two-dimensional diagnostic model (Bi and Zhao, 1993). Using a three-dimensional nonlinear numerical model, Liu et al. (2003) also suggested that upwelling appears around all fronts in the YS and accounts for SCPs near the frontal area.

A recent hydrological investigation also indicated the existence of frontal upwelling offshore of the Subei Bank and Shandong Peninsula (Yuan et al., 2017). Based on a three-dimensional, wave–tide–circulation coupled numerical model, Lü et al. (2010) demonstrated that the upwelling in the YS is largely induced by the tidal mixing front over the sloping topography, and the large temperature difference across the front leads to a strong baroclinic pressure gradient force in the bottom layer, which triggers upwelling in the bottom layer and downwelling in the upper layer.

Previous studies have mainly focused on the distribution and formation mechanism of frontal upwelling in the YS. However, the factors influencing frontal upwelling strength have rarely been studied. In this study, a three-dimensional hydrodynamic model is applied to solve this problem. The remainder of this paper is organized as follows. In Section 2, observational data and the model configuration as well as its validation are presented. In Section 3, a series of numerical experiments are performed to estimate the effects of several local factors on the intensity of frontal upwelling. Then, the influencing mechanism of the key factors is investigated in Section 4. Finally, conclusions are drawn in Section 5.

2 Data and model

2.1 *Observational data*

Cruise observations were conducted in the western YS during August 19–27, 2015. The cruises covered the sea region west of 124°E, from 32°N to 38.75°N. During this period, there was no tropical cyclone passing over the YS. The temperature was obtained by a SeaBird 911 conductivity-temperature-depth (CTD) profiler and calibrated by SeaBird software with an accuracy of 0.001°C. The CTD investigation was performed along zonal sections in the southwestern YS. Except for the Changjiang River Estuary and Dalian–Chengshanjiao sections, the spatial resolution of most CTD stations was 0.5° in the zonal direction and 1° in the meridional direction. The locations of the CTD stations for the August 2015 cruise are presented in Fig. 1b.

The current measurements were obtained from a mooring Acoustic Doppler Current Profiling (ADCP) located in the western YS (34°N, 122.75°E); the location of the mooring station is presented in Fig. 1b. The ADCP was located at a depth of 44 m with a vertical resolution of 2 m. The observations were conducted from April 8 to October 19, 2015, with a sampling interval of

30 min. To ensure the reliability of the ADCP data, the internal compass was calibrated before launching the ADCP. In addition, the data underwent quality control before analysis, including assessment of horizontal and vertical velocity, percentage of good pings, pitch and roll, echo intensity, correlation magnitude, velocity error, side lobe effects, etc. Ensembles with a percentage of good pings less than 90 were removed. In addition, the first two layers of data (the blind district of the ADCP), data with velocities greater than 2 m/s, and data within 5 m below the sea surface (affected by bubbles and side lobes) were also removed.

Furthermore, a harmonic analysis, which was developed to extract tidal signals from ADCP data, was applied to obtain the tidal currents. When did harmonic analysis of tidal current, eight tidal constituents (M_2, S_2, K_1, O_1, N_2, K_2, P_1, and Q_1) were adopted, because the time series were long enough (1 month of data with a sampling interval of 30 min), all tidal constituents were extracted successfully, and the total variance of the predicted values accounted for 97.2% of the observed values.

2.2 *Model description and configuration*

A high-resolution regional circulation model based on the Regional Ocean Modeling System is adopted for the study region. The model covers a domain of 22°–42°N, 117°–140°E with a horizontal resolution of (1/18)°×(1/18)° (Fig. 1a). We adopt a 32-level stretched generalized terrain-following coordinate. For the vertical mixing parameterization, the local closure scheme of Mellor and Yamada (1982) is applied, which is based on the level 2.5 turbulent kinetic energy equations.

The model is driven by the daily wind speed, longwave and shortwave radiation, air temperature, sea level pressure, precipitation, evaporation, and relative humidity, which were provided by the European Centre for Medium-Range Weather Forecasts (ECMWF) through the Interim ECMWF re-analysis dataset with a horizontal resolution of 0.25°. The sea surface temperature (SST) was obtained from Optimum Interpolation Sea Surface Temperature v2.1 with a horizontal resolution of 0.25°, which was supplied by the National Ocean and Atmosphere Administration. Based on these data, the momentum, surface heat and salt fluxes were calculated using bulk formulae (Fairall et al., 2003). The climatological mean sea surface salinity was taken from World Ocean Atlas 2013 (WOA13), and the horizontal resolution from WOA13 was 0.25°. All input forcing datasets are interpolated on the model grid. The monthly mean discharge of the Changjiang River in the model was measured by the Changjiang Water Resource Commission at Datong Station (http://www.cjw.gov.cn/).

The lateral open boundary is forced by monthly means of subtidal sea surface height, velocity, temperature and salinity. Both the boundary data and initial conditions were obtained from the Simple Ocean Data Assimilation (Carton et al., 2018). The tidal forcings with four main harmonic constituents (M_2, S_2, K_1, and O_1), which are the most dominant contributors in the YS, are applied to the lateral boundary. The tidal components were derived from the TPXO7 ocean tidal model.

The model is run for 15 years from January 1, 2001 to December 31, 2015. The last 10 years (from 2006 to 2015) are averaged to obtain the climatological upwelling conditions.

2.3 *Validation of tidal elevations and currents*

Considering the important role that tides play in the YS, the simulated tide is first compared with the observations. The model is run in barotropic mode (setting the temperature to 15°C and salinity to 35) with only tidal forcings added at open boundaries. The modelled co-tidal charts of the M_2 constituent (Fig. 2a) show good agreement with previous studies (Wan et al., 1998; Fang et al., 2004; Zhang et al., 2005). Two amphidromic points in the YS are located offshore of Chengshanjiao and Haizhou Bay.

In addition, the harmonic constants of the modelled M_2 tide are compared with the observed values (Figs 2b, c). The observed data were derived from 77 tide gauges (shown in Fig. 2a) provided by Wan et al. (1998). The correlation coefficients

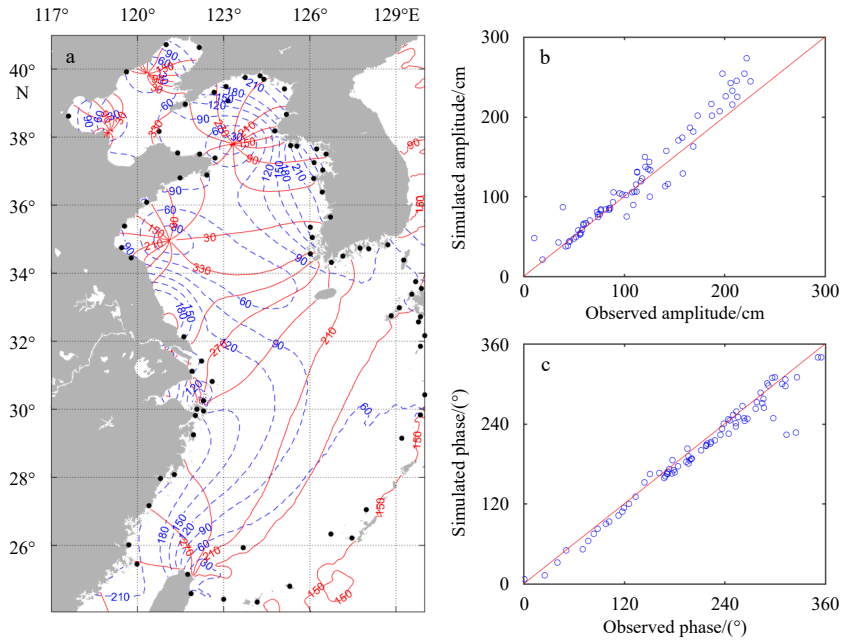

Fig. 2. M_2 co-tidal chart simulated by the model with homogeneous water; the solid and dashed lines denote the phase lag (°) and amplitude (cm), respectively; the phase lag was referenced to Beijing local time (UT + 8 h); the black dots denote locations of 77 tide gauges (a); comparison between the modelled and observed amplitudes at 77 tidal gauges represented by the dots in a (b); c is same as b but for the phase lag.

between the observed and modelled tidal amplitudes and phases are 0.97 and 0.98 (at the 95% confidence level), respectively, with root mean square errors of 22.5 cm and 16.8°, respectively. The comparison suggests a generally satisfactory reproduction of the M_2 tide by the model.

Furthermore, the simulated tidal currents are compared with the observed data at the H05 mooring station (Fig. 3). For the depth-mean tidal current, the correlation coefficient between the observed and modelled meridional velocity is 0.94 at the 95% confidence level, and the root mean square error is 0.1 m/s. Similarly, the correlation coefficient between the observed and modelled zonal velocity is 0.97 at the 95% confidence level, with a root mean square error of 0.04 m/s.

2.4 *Validation of temperature*

To examine whether the model results are able to capture the hydrographic features of the YS, the monthly mean Moderate Resolution Imaging Spectroradiometer (MODIS) SST datasets (https://modis.gsfc.nasa.gov/), with a horizontal resolution of 4 km, are selected for comparison with the model results in August 2015 (Fig. 4). SCPs are easily identified near the coast of the YS, especially offshore Liaodong Peninsula, east of Chengshanjiao on the Shandong Peninsula, Haizhou Bay, Subei Bank, Korean Bay, Kyunggi Bay and offshore Mokpo. Both the MODIS SST and model results show that the temperature in these regions is 2–5°C lower than that in the surrounding waters. The SCPs are stronger near the eastern coast of the YS than the western coast.

The model results match the MODIS SST well; however, there are still some distinctions between them. For example, the area of SCPs offshore Liaodong Peninsula in the model results is larger than that in the MODIS SST, which may be due to the overestimation of the advection effect of the YSCWMC in the model, which could transport cold water from north to south.

In addition, the CTD data conducted in August 2015 are selected to validate the model results (Fig. 5). In summer, the YSCWM is characterized by three cold cores located in the northern, southeastern and southwestern YS, respectively (Fig. 5b), which is in agreement with Weng et al. (1989) and Yu et al. (2006). The northern and southeastern cores are stronger (colder), with the lowest temperatures lower than 6°C, while the southwestern core is weaker (warmer), with temperatures between 8°C and 10°C. Along the boundary of the YSCWM, strong bottom temperature fronts (BTFs) separate the cold water on the offshore side from the warm water on the other side. It should be noted that the simulated BTFs are much stronger than the observations, which may be due to the low resolutions (approximately 0.5° in the zonal direction and 1° in the meridional direction) of the CTD stations.

The distribution of bottom temperature is closely related to

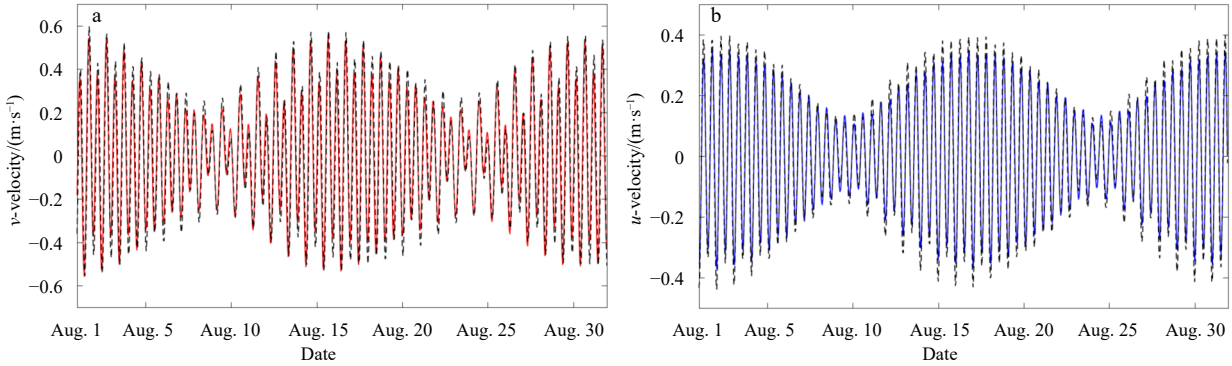

Fig. 3. Comparisons between observed (solid lines) and modelled (dashed lines) results for meridional (a) and zonal (b) depth-mean tidal velocities at the H05 mooring station (shown in Fig. 1b).

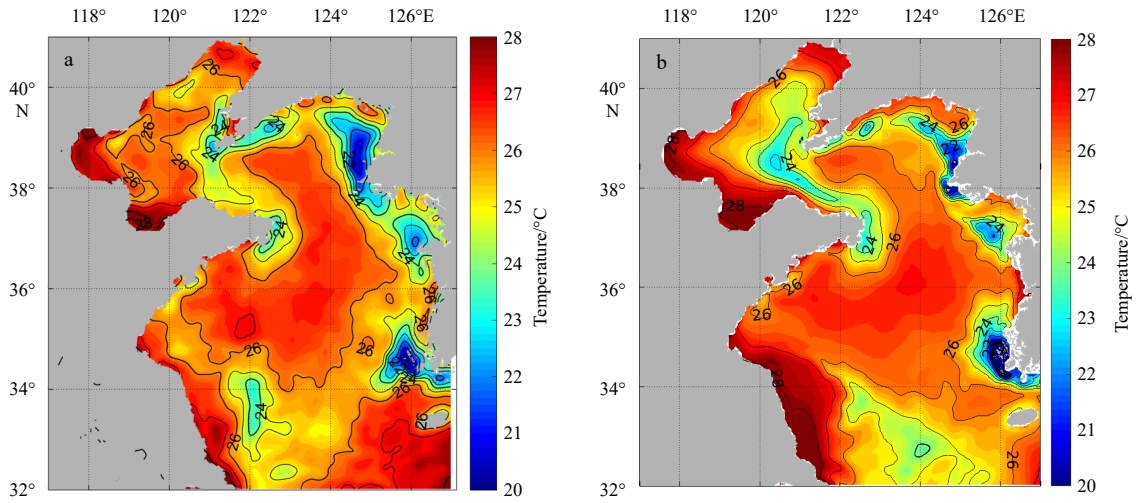

Fig. 4. Horizontal distribution of the monthly mean sea surface temperature in the Moderate Resolution Imaging Spectroradiometer (a) and model results (b) in August 2015.

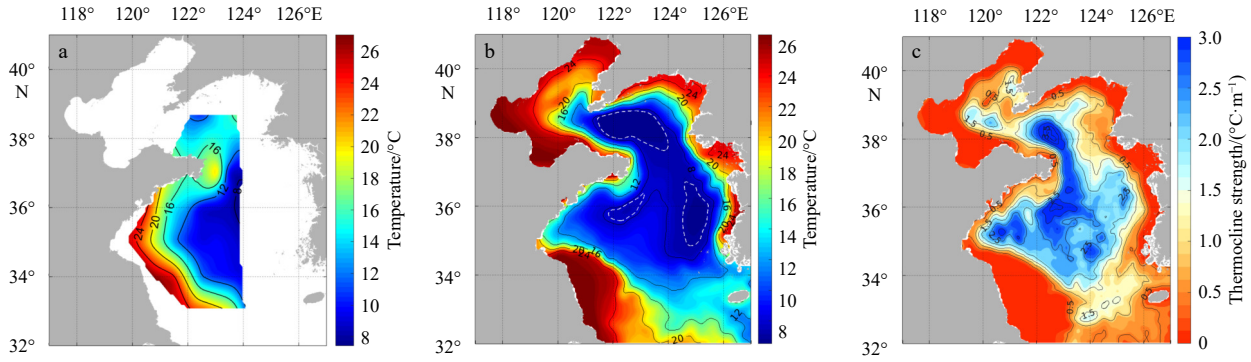

Fig. 5. Bottom temperature distribution of *in situ* observations (a) and monthly mean model results (b) in August 2015. The contour interval (CI) is 4°C. White dashed lines denote three cold cores of the Yellow Sea Cold Water Mass. c. Distributions of thermocline strength in August 2015. Unit: °C/m with CI=0.5°C/m.

the thermocline of the YS. In the shallow region, the water is well mixed due to surface waves and tidal mixing (Qiao et al., 2006). However, in the offshore region, the sea is strongly stratified in the upper layer due to surface heating. To further explore the relationship between the thermocline and bottom temperature, we calculated the maximal vertical temperature gradient as the thermocline strength of the YS. The results show that the thermocline is strong in the central YS but much weaker in the coastal water (Fig. 5c), which causes the bottom water to be warmer near the coast but much colder in the trough. The distribution of the thermocline strength is in agreement with Ge et al. (2006).

Figure 6 shows the temperature distribution along 35°N and 36°N in August. The front and thermocline block the YSCWM at the bottom of the YS, with an envelope line of 10°C. In the frontal area, the isotherm is generally convex and even crops out at the sea surface, which induces SCPs there. In the middle of the YS, the residual water of the Yellow Sea Warm Current, which is warmer and saltier than the surrounding water, separates the YSCWM into western and eastern cores (Xia et al., 2004; Yu et al., 2006).

The comparison between the simulated and observed data shows that the basic temperature distributions of the YS are well represented by the model. However, some defects still persist in the model results; for instance, the thickness of the upper mixed layer is underestimated by simulations (Fig. 4), which may be caused by insufficient surface wave mixing (Qiao et al., 2006; Lü et al., 2010).

3 Results

3.1 *Horizontal distribution of frontal upwelling*

Based on multiple years (2006–2015) of model results, the distribution of climatological upwelling velocity at the bottom of the YS in August is shown in Fig. 7a. Upwellings widely occur in the coastal shallow waters of the YS. The upwelling is stronger near the coast of Korea, with the maximum velocity exceeding 5×10^{-5} m/s; conversely, upwelling near the coast of China is weaker. The distribution of upwelling is in accordance with the SCPs (Fig. 4), both of them are mainly located in offshore Liaodong Peninsula, east of the Shandong Peninsula, Subei Bank and Korean Peninsula.

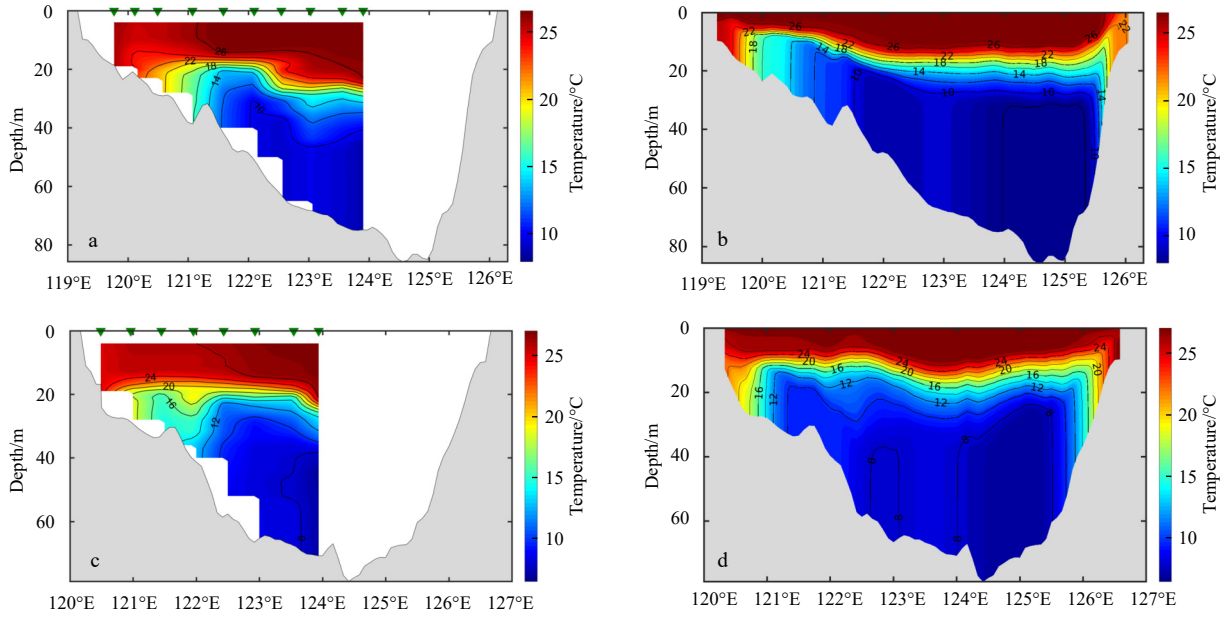

Fig. 6. Temperature distributions of *in situ* observations (a, c) and monthly mean model results (b, d) in August 2015. The upper panels represent the 35°N section, and the lower panels represent the 36°N section. The contour interval is 4°C. The triangles in a and c denote the conductivity-temperature-depth stations.

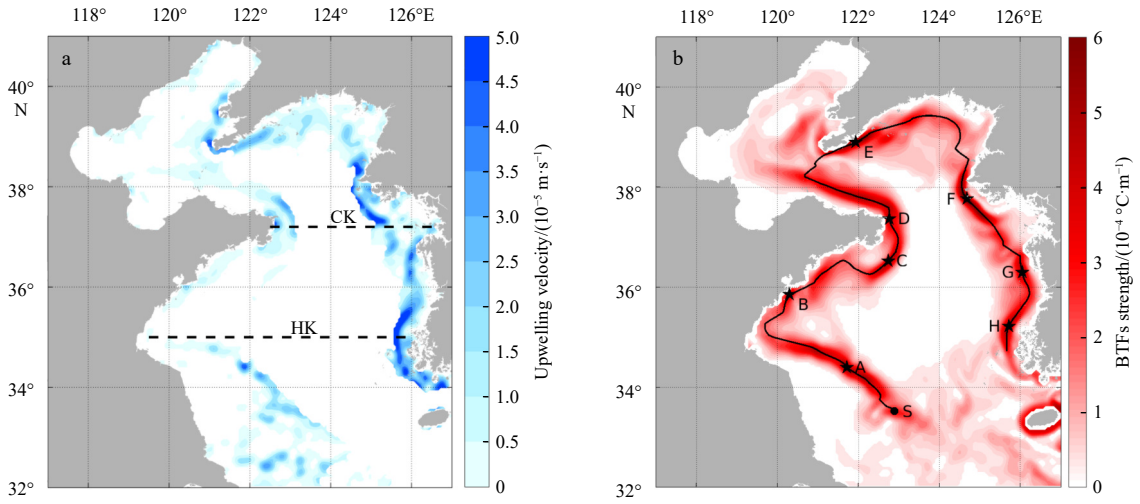

Fig. 7. Horizontal distributions of simulated bottom upwelling velocity (a); the dashed lines show two representative sections along 35°N (HK) and 37.2°N (CK); simulated bottom temperature fronts (BTFs) in August (b); the thick solid line denotes the location of the maximum temperature gradient along the belt of BTFs; S denotes the starting point of the solid line; A–H represent locations of maximum values in Fig. 6.

Furthermore, to better understand the relationship between upwellings and BTFs, the bottom temperature gradient (BTG) is calculated using the following equation:

$$\mathrm{BTG} = \sqrt{(\partial T/\partial x)^2 + (\partial T/\partial y)^2}, \tag{1}$$

where T denotes the bottom temperature. We choose 3×10^{-5} °C/m as the critical value of the BTFs according to Liu and Wang (2009); then, the distribution of the BTFs is obtained, as shown in Fig. 7b. The BTFs mainly lie in the coastal YS, with the maximum value exceeding 6×10^{-4} °C/m, which envelops the YSCWM and induces strong baroclinicity near the frontal area. The distribution of BTFs highly coincides with that of upwellings; both BTFs and upwelling are strong near the boundary of the YSCWM and weak in the interior area. Lü et al. (2010) suggested that strong baroclinicity near the frontal area is the leading cause of frontal upwelling.

The strength of BTFs and upwelling along the coast of the YS (the solid line in Fig. 7b) are represented in Fig. 8 and show significant regional characteristics. Both of them reach extreme values in the offshore regions of (A) Subei Bank, (B) Qingdao, (C–D) Chengshanjiao, (E) Liaodong Peninsula, (F) north of Kyunggi Bay, (G) Boryeong and (H) Mokpo (the positions of A–H are shown in Fig. 7b). Among these positions, the frontal strength is maximal in northern Kyunggi Bay (7.1×10^{-4} °C/m) and minimal in Haizhou Bay (3.9×10^{-4} °C/m). Similarly, the mean upwelling velocity is much stronger on the eastern coast of the YS (approximately 3.32×10^{-5} m/s) than on the western coast (approximately 1.16×10^{-5} m/s).

The coefficient of the correlation between BTF strength and upwelling velocity is 0.62 in the eastern YS and 0.5 in the western YS, both of them passes significance inspection at the 95% confidence level, which indicates that the BTFs have a certain effect on not only the distribution but also the strength of the upwelling.

Many previous studies have revealed that tidal forcings give rise to the formation of BTFs and related upwellings (Zhao, 1986, 1987b; Lü et al., 2010). Our study further indicates that tidal forcings dominate the semi-monthly variation in bottom upwelling

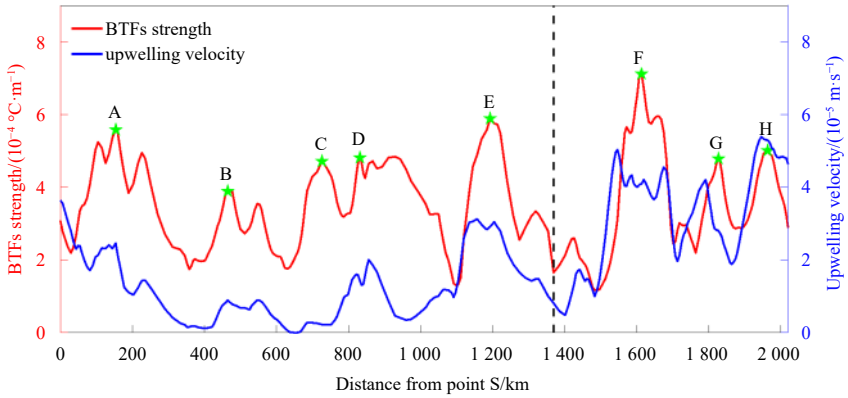

Fig. 8. The distributions of bottom temperature fronts (BTFs) strength and upwelling velocity along the slope of the Yellow Sea (YS) (the thick solid line in Fig. 7b) in August. The green stars denote the maximum values in different regions. The locations of A–H are presented in Fig. 7b. The dashed line denotes the location of 124°E, which was selected as the divide between the western YS and eastern YS.

strength (Fig. 9). Accompanied by periodic changes in tidal forcings, upwelling shows a significant spring-neap tidal variation in the YS. During neap tidal phases, the average intensity of bottom upwelling is approximately 2×10^{-5} m/s. However, the strength doubles to more than 4×10^{-5} m/s during spring tidal phases.

The analysis above indicates that upwellings widely exist in the frontal area of the YS, and the strength and distribution of the upwelling show significant regional characteristics and largely depend on the BTFs. Strong upwelling always occurs in the strong frontal area and is conducive to forming SCPs.

3.2 *Key factors influencing the upwelling intensity*

3.2.1 *Effects of shelf slope on the upwelling strength*

A characteristic bathymetric feature of the YS is the trough that extends northwestward along the east-central YS, which causes a much steeper slope on the eastern coast and a gentler slope on the western coast. The analysis above also shows that the upwelling in the eastern YS is much stronger than that in the western YS. To investigate the effects of the shelf slope on the upwelling strength, the shelf slopes in the western and eastern YS are set to be identical by setting symmetrical bathymetry in the sensitivity experiment (ExpA). The distribution of the bathymetry in the control run and ExpA is shown in Fig. 10.

The vertical circulation along 35°N (HK section represented in Fig. 7a) is selected to analyse the difference in ExpA (Fig. 11). In the control run, the upwelling is strong along the steep slope on the eastern side of the YS, which brings cold water from the bottom to the upper layer and even reaches the surface of the sea (Fig. 11a); consequently, the thermocline tilts up and ventilates at the sea surface, and the SCPs thus develop offshore of Mokpo (Fig. 4b). However, the upwelling is much weaker and broader on the western side of the YS; as a result, the SCPs in Haizhou Bay are much weaker than those offshore Mokpo.

In ExpA, the bathymetry is set to be symmetrical, and the shelf slope is set to be identical. The double cold cores of the YSCWM disappear in the centre of the YS (Fig. 11b); furthermore, the front near the eastern coast becomes broader and weaker. As a result, the upwelling near the eastern coast is much weaker than that in the control run. In contrast, the upwelling near the western coast in ExpA becomes stronger.

The results show that the shelf slope not only influences the temperature structure but also has a significant effect on the upwelling strength. A steeper slope is more conducive to generating a stronger front and upwelling; in contrast, upwelling along a gentler slope is more likely to be weaker and broader.

3.2.2 *Effects of external forcings on the upwelling strength*

Previous studies have indicated that the local wind, topography and stratification have certain impact on the upwelling

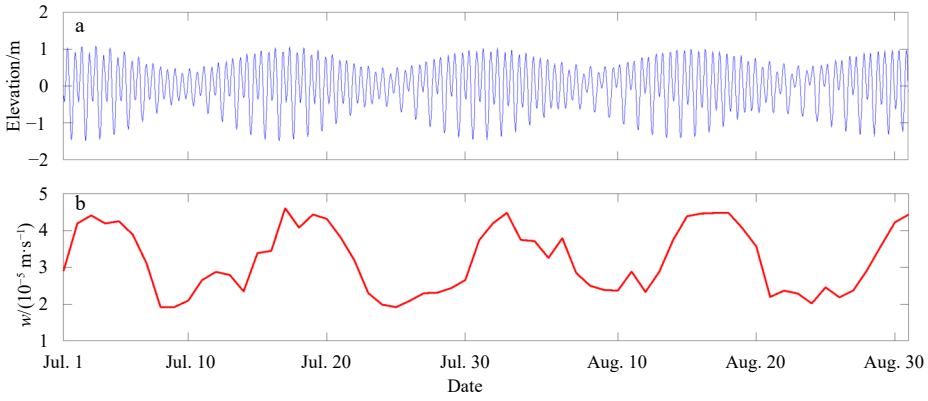

Fig. 9. Time series of modelled surface elevation at the H05 mooring station for July and August 2015 (a); time series of bottom upwelling strength (w) averaged from points A–H (b).

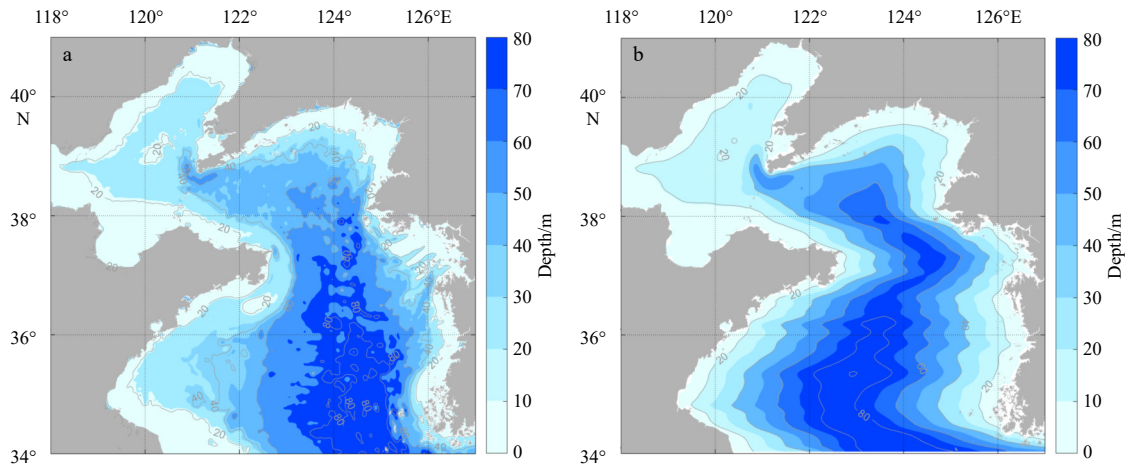

Fig. 10. Distributions of the topography in the control run (a) and ExpA (b); the topography was set to be symmetrical in the southern Yellow Sea. The coloured shading and grey solid lines denote bathymetry (in m), contour interval=20 m.

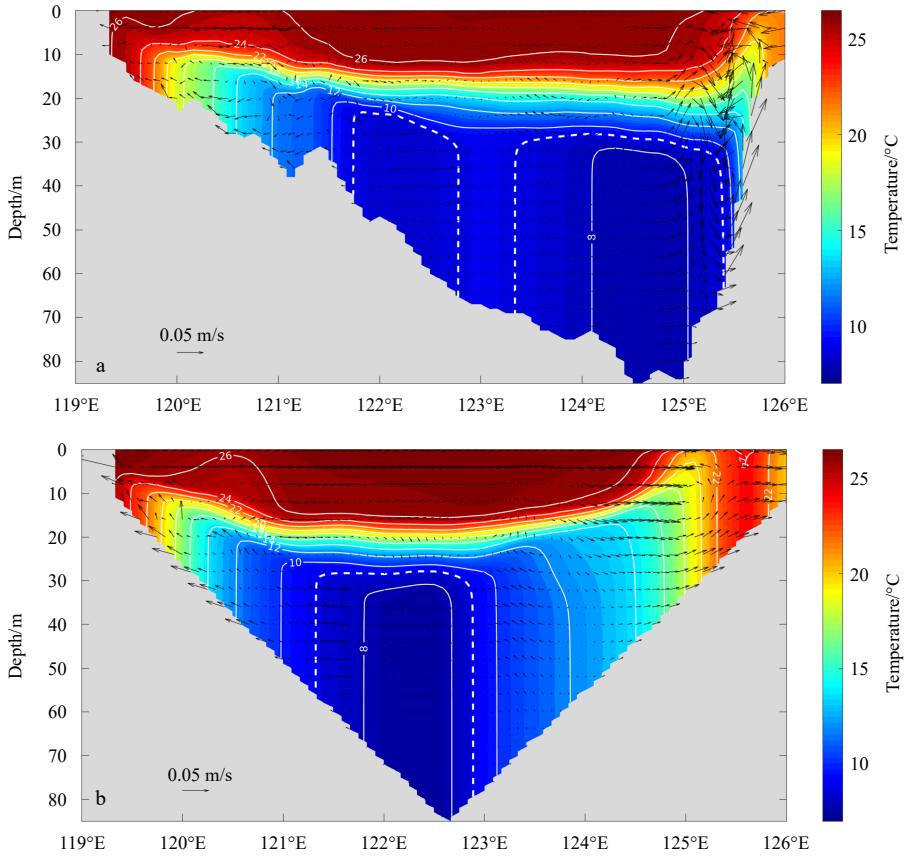

Fig. 11. Distributions of temperature and *u*-*w* velocity along the 35°N section in the control run (a) and ExpA (b). The coloured shading and white solid lines denote temperature in °C, the white dashed lines denote cold cores of the Yellow Sea Cold Water Mass. Vectors denote *u*-*w* velocity, and the vertical velocity has been multiplied by 1 000.

intensity in the northern South China Sea (Wang et al., 2012, 2014; Shu et al., 2018a, 2018b). However, how external forcings influence the intensity of upwelling in the YS has rarely been investigated. Our analysis above suggests that the upwelling strength is largely determined by the BTFs; moreover, the difference in air temperature between summer and the previous winter could influence the strength of BTFs (Guan, 1963). Thus, we infer that external forcings may influence the intensity of frontal upwelling by changing the strength of BTFs.

To verify our conjecture, several numerical experiments are designed based on the reference month of August 2015. The results for August 2015 are set as the control run (ctl). In each experiment, the air temperature, southerly wind, and precipitation rate are increased by 20% in the previous winter, spring and summer, respectively (Table 1). The change ratios of frontal upwelling in each experiment are analysed.

To quantify the influence of external forcings on frontal upwelling, the change ratio (α) of frontal upwelling in each experiment is calculated as follows:

$$\alpha = \frac{S_{\mathrm{exp}} - S_{\mathrm{ctl}}}{S_{\mathrm{ctl}}} \times 100\%, \tag{2}$$

where S_{exp} and S_{ctl} represent the upwelling strength in the experiment group and control group, respectively. The average change ratio in the entire YS (α_{A}) and the average change ratio in the western (α_{W}) and eastern (α_{E}) YS are calculated using the following formula, respectively:

Table 1. Changes in external forcings in sensitivity experiments

Experiment	Forcing conditions
Expt1	air temperature in the previous winter increased by 20%
Expt2	air temperature in spring increased by 20%
Expt3	air temperature in summer increased by 20%
Expw1	southerly wind in the previous winter increased by 20%
Expw2	southerly wind in spring increased by 20%
Expw3	southerly wind in summer increased by 20%
Expr1	precipitation rate in the previous winter increased by 20%
Expr2	precipitation rate in spring increased by 20%
Expr3	precipitation rate in summer increased by 20%

Note: The previous winter is defined as December to February, springis defined as March to May, and summer is defined as June to August.

$$\alpha_{\mathrm{A}} = \frac{\sum_{i=1}^{k} \alpha_i}{k}, \quad \alpha_{\mathrm{W}} = \frac{\sum_{i=1}^{m} \alpha_i}{m}, \quad \alpha_{\mathrm{E}} = \frac{\sum_{i=1}^{n} \alpha_i}{n}, \tag{3}$$

where k denotes the model grid of the entire region of the YS. In addition, the longitude 124°E is selected as the division line of the western YS and eastern YS; thus, m denotes the model grid west of 124°E, and n is the model grid east of 124°E.

The results show that the southerly wind speed and air temperature in summer, as well as the air temperature in the previous winter and spring, significantly impact the strength of frontal upwelling (Fig. 12). Among these forcings, the meridional wind

speed in summer is the primary factor. When the southerly wind in summer is increased by 20%, the frontal upwelling in the western YS strengthens by 17.71%; however, the upwelling in the eastern YS weakens by 11.79%.

The secondary factor is the air temperature in summer, followed by the air temperature in the previous winter and spring. When the air temperature in summer is increased, the frontal upwelling in both the western and eastern YS strengthens, with change ratios of +11.05% and +4.4%, respectively. However, when the air temperature in the previous winter and spring is increased, the frontal upwelling in the YS weakens, with change ratios of –3.47% and –2.41%, respectively, which are smaller than those in summer. The influence of precipitation is inappreciable, with change ratios less than 1% (not shown), which can be neglected.

Figure 13 shows the horizontal distribution of the change in magnitude of frontal upwelling in Expt1–Expt3 and Expw3. The results also indicate that an increase in air temperature in the previous winter and spring weakens frontal upwelling in summer (Figs 13a, b); in contrast, an increase in air temperature in summer strengthens frontal upwelling (Fig. 13c). When the southerly wind in summer increases, the upwelling intensifies in the western YS and weakens in the eastern YS (Fig. 13d).

4 Discussion

Since the southerly wind speed and air temperature in summer and the air temperature in the previous winter and spring play significant roles in the intensity of frontal upwelling, the influencing mechanisms of these factors are analysed in this section.

The winter process is considered as the key factor influencing the temperature of the bottom water in the YS in summer (Guan, 1963; Zhang and He, 1989; Jiang et al., 2007; Oh et al., 2013; Yang et al., 2014; Li et al., 2015; Zhu et al., 2018). During winter, the entire water column of the YS mixes homogenously due to the strong wind stirring and surface cooling (He et al., 1959), and atmospheric signals can be transmitted throughout the water column. When the air temperature in the previous winter increases, the warm anomaly is transmitted to the bottom of the YS. From spring to summer, the warm anomaly gradually vanishes in the shallow region (Fig. 14a) due to the strong mixing induced by tidal forcing and wind stirring (Qiao et al., 2006). However, in the offshore region, the warm anomaly is preserved due to the strong stratification (Fig. 5c).

To quantify the effect of the vertical mixing process on the variation of bottom temperature anomaly, the vertical diffusion term (VDIF) from February to August 2015 is calculated as follows:

$$\mathrm{VDIF} = \sqrt{\mathrm{VDIF}_u^2 + \mathrm{VDIF}_v^2}, \tag{4}$$

where VDIF_u and VDIF_v denote the vertical diffusion term for u and v, respectively, which are calculated using following formula:

$$\mathrm{VDIF}_u = \frac{\partial}{\partial z}\left(K_\mathrm{v}\frac{\partial u}{\partial z}\right),\ \mathrm{VDIF}_v = \frac{\partial}{\partial z}\left(K_\mathrm{v}\frac{\partial v}{\partial z}\right), \tag{5}$$

where K_v represents vertical eddy viscosity, and u and v represent the zonal and meridional velocity, respectively. The time variation in VDIF along the bottom of the 36°N section is shown in Fig. 14b. The results show that the vertical mixing is much stronger along the coast of the YS than in the trough. In addition, from winter to summer, the strong mixing is sustained in the coastal region and attenuates the warm anomaly there; however, in the offshore region, the warm anomaly does not change much because of the weak mixing. This attenuates the BTFs (Fig. 15a), and frontal upwelling thus slackens due to the weakened baroclinicity.

The results of Expt2 show a similar pattern to Expt1; however, they show smaller magnitudes of the warm anomaly and lower change ratios (Fig. 15b), this is because the stratification begins to form in spring, which restricts the downward transfer of surface heat. When the air temperature in summer increases, the coastal water warms rapidly; however, the bottom water in the central YS does not change much due to the strong stratification (Fig. 5c), which strengthens the BTFs (Fig. 15c) and consequently enhances the frontal upwelling due to the intensified baroclinicity.

When the southerly wind in summer intensifies, the bottom temperature decreases in the western frontal area but increases on the eastern coast (Fig. 15d). This is in accord with the upwelling anomaly in Fig. 13d. The strengthened upwelling in the western YS brings more cold water from the YSCWM to the coastal region along the slope, which makes it colder on the western coast of the YS; in contrast, the attenuated upwelling in the

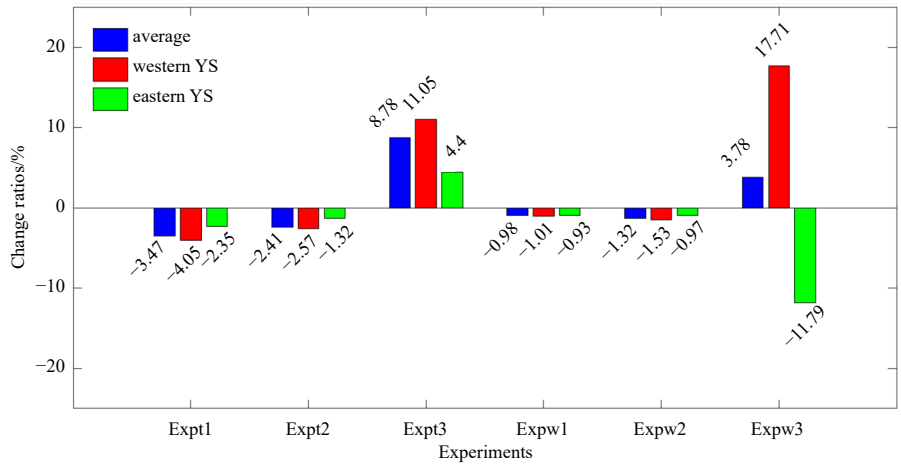

Fig. 12. Regional average change ratios in frontal upwelling in each experiment. The longitude 124°E was selected as the division line of the western Yellow Sea (YS) and eastern YS.

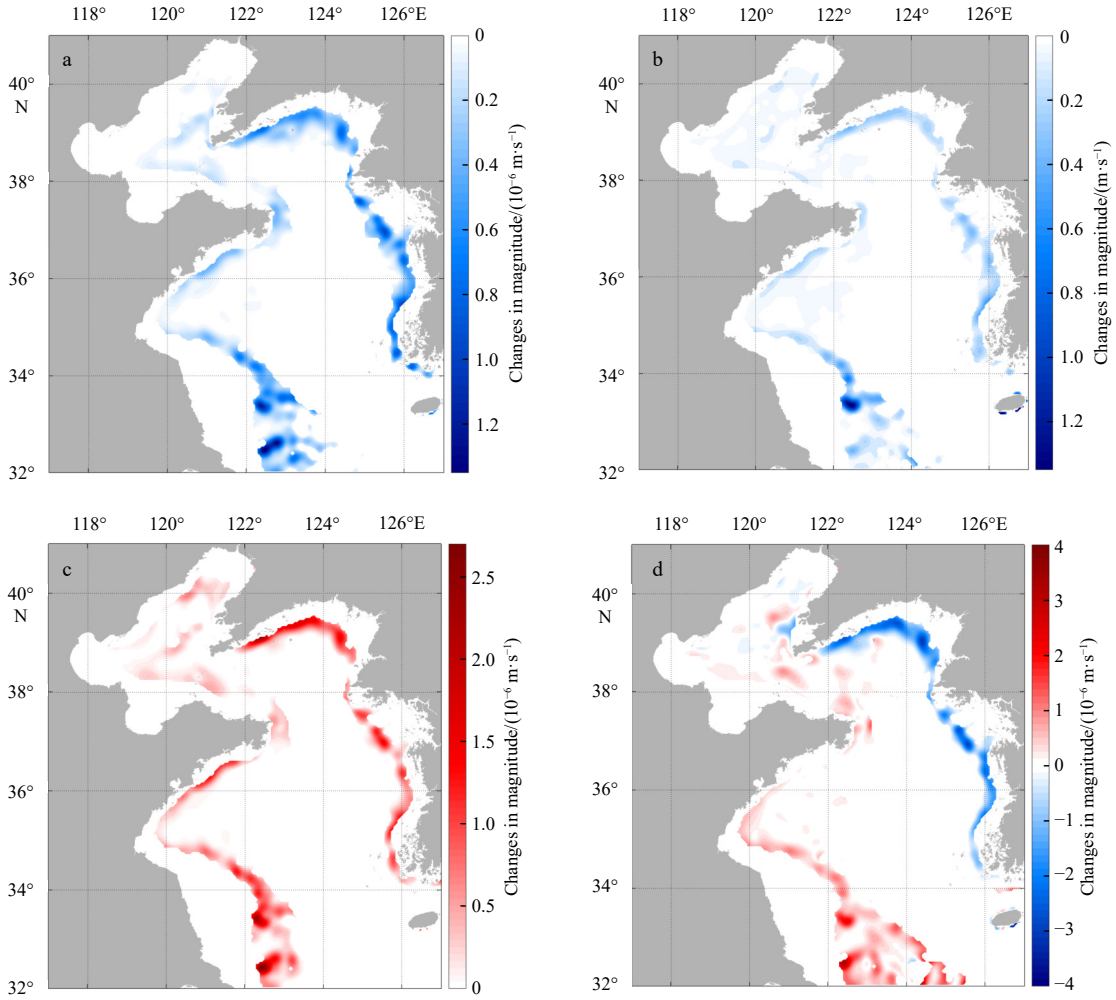

Fig. 13. Distribution of the change in magnitude of upwelling in Expt1 (a), Expt2 (b), Expt3 (c) and Expw3 (d).

eastern YS makes the bottom water warmer on the eastern coast.

To further explore the influence mechanism of the southerly wind in summer, the *u*-*w* anomalies along the 35°N section (HK section in Fig. 7a) and 37.2°N section (CK section in Fig. 7a) in Expw3 are analysed (Fig. 16). In Expw3, the strengthened southerly wind drives more surface water to the east due to the Ekman effect, and the sea surface water thus converges near the eastern coast of the YS and induces a downwelling anomaly in the frontal region. Similarly, the offshore current anomaly near the western coast leads to the divergence of sea surface water and drives an upwelling anomaly along the slope of the western YS. As a result, the upwelling strengthens in the western YS and weakens in the eastern YS due to Ekman pumping.

It should be noted that the southerly wind prevails in summer in the YS, which is conducive to offshore Ekman transport and triggers upwelling along the western coast. Thus, the upwelling in the western YS is the joint effect of the tidal mixing front and Ekman transport.

The mechanism analysis indicates that the air temperature could influence the strength of the frontal upwelling by changing the baroclinicity in the frontal region. At the same time, the meridional wind speed in summer could affect frontal upwelling via

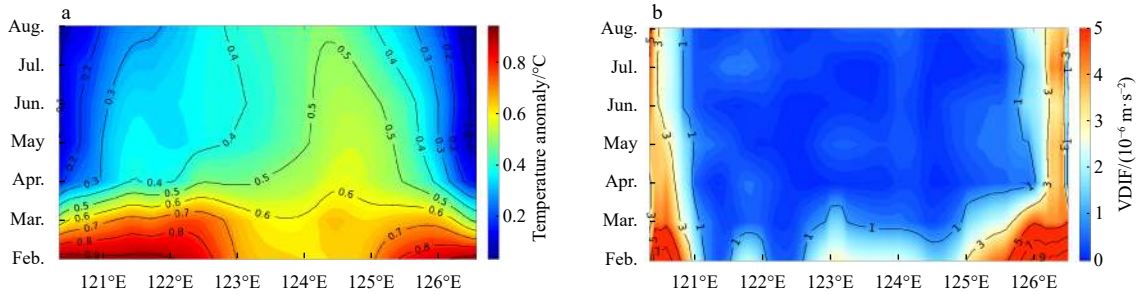

Fig. 14. Time variations of the temperature anomaly in Expt1 (a) and the vertical diffusion term (VDIF) in the control group (b) along the bottom of the 36°N section from February to August 2015.

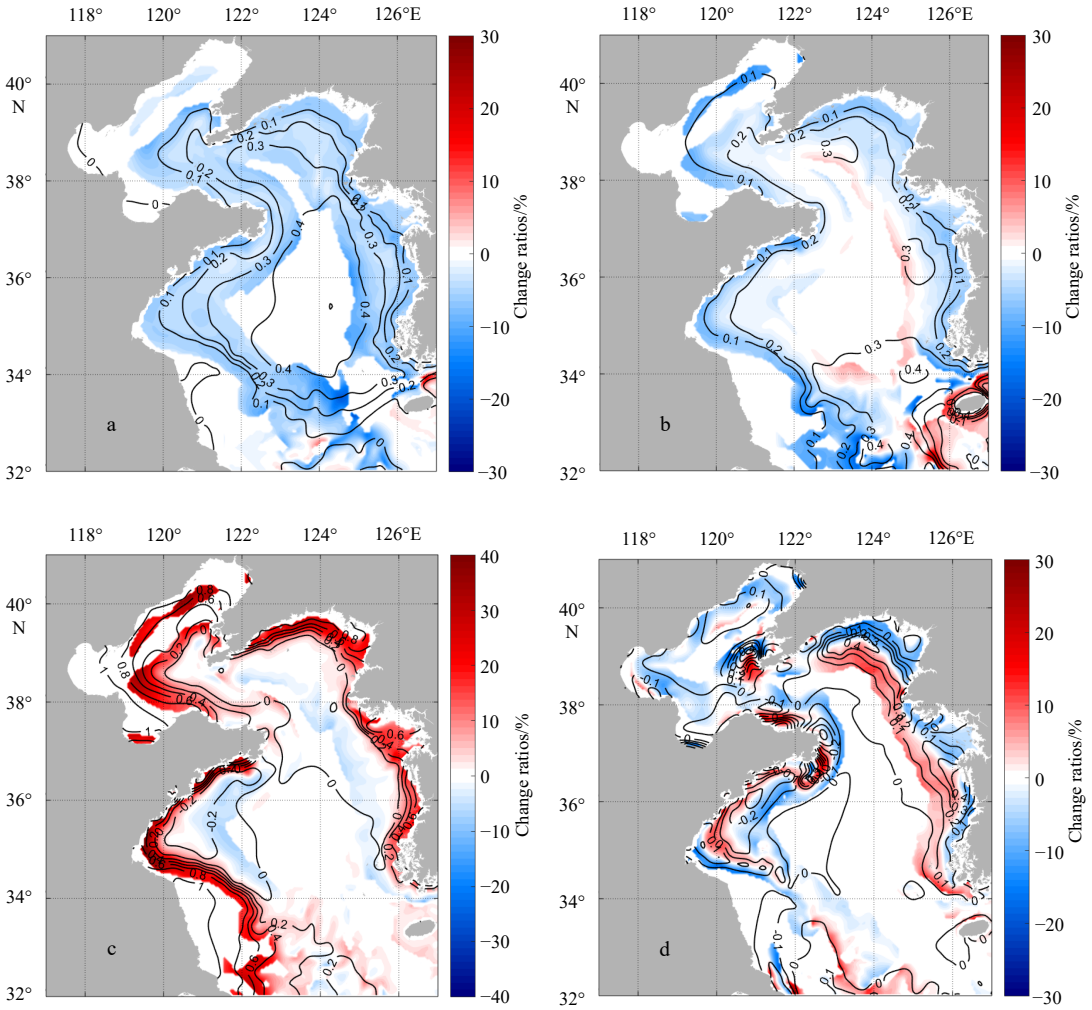

Fig. 15. Horizontal distributions of the bottom temperature anomaly (solid lines, unit: °C) and change ratio of the bottom temperature gradient (coloured shading) in Expt1 (a), Expt2 (b), Expt3 (c) and Expw3 (d).

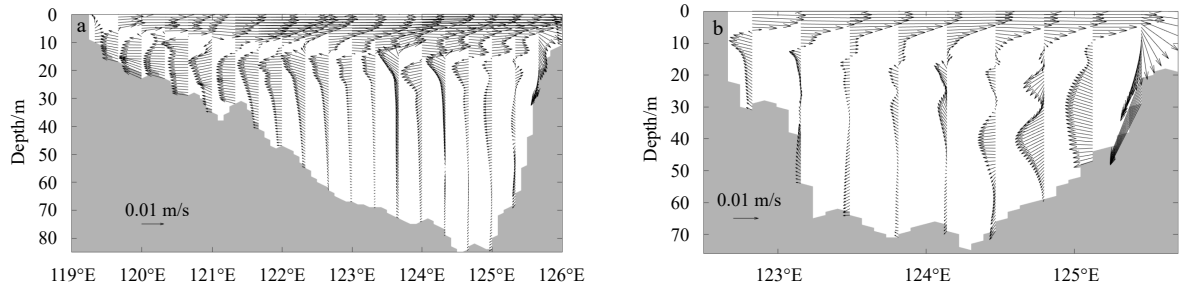

Fig. 16. Distributions of *u*-*w* anomalies along the 35°N section (a) and 37.2°N section (b) in August in Expw3. The vertical velocity has been multiplied by 1 000.

Ekman pumping.

5 Conclusions

A three-dimensional hydrodynamic model is applied to study the characteristics and influencing factors of frontal upwelling in the YS. The results indicate that upwellings widely exist in the frontal area of the YS, which shows significant regional characteristics and is largely dependent on the BTFs.

Sensitivity experiments show that both topography and external forcings have certain effects on the strength of frontal upwelling. A steeper slope is more conducive to generating a stronger front and upwelling; in contrast, upwelling along a gentler slope is more likely to be weaker and broader.

Furthermore, the meridional wind speed and air temperature in summer, as well as the air temperature in the previous winter and spring, have certain impacts on the strength of frontal upwelling. When the southerly wind in summer strengthens, more surface water is driven to the eastern coast of the YS; as a result, the upwelling intensifies in the western YS and weakens in the eastern YS. When the air temperature in the previous winter and

spring increases, the warm anomaly is preserved in the YSCWM, which causes the weakening of the BTFs and frontal upwelling. In contrast, when the air temperature in summer increases, the shallow water near the coast of the YS warms rapidly, which intensifies the BTFs and associated upwelling.

Acknowledgements

We thank the technology support provided by High Performance Computing Center, Institute of Oceanology, Chinese Academy of Sciences.

References

Beardsley R C, Limeburner R, Kim K, et al. 1992. Lagrangian flow observations in the East China, Yellow and Japan Seas. La mer, 30(3): 297–314

Bi Yawen, Zhao Baoren. 1993. Numerical simulation of cross front in the shelf front area of south-western Yellow Sea. Marine Sciences, (6): 61–64

Carton J A, Chepurin G A, Chen Ligang. 2018. SODA3: a new ocean climate reanalysis. Journal of Climate, 31(17): 6967–6983, doi: 10.1175/JCLI-D-18-0149.1

Fairall C W, Bradley E F, Hare J E, et al. 2003. Bulk parameterization of air–sea fluxes: Updates and verification for the COARE algorithm. Journal of Climate, 16(4): 571–591, doi: 10.1175/1520-0442(2003)016<0571:BPOASF>2.0.CO;2

Fang Guohong, Wang Yonggang, Wei Zexun, et al. 2004. Empirical cotidal charts of the Bohai, Yellow, and East China Seas from 10 years of TOPEX/Poseidon altimetry. Journal of Geophysical Research: Oceans, 109(C11): C11006, doi: 10.1029/2004JC002484

Feng Ming, Hu Dunxin, Li Yongxiang. 1992. A theoretical solution for the thermohaline circulation in the southern Yellow Sea. Chinese Journal of Oceanology and Limnology, 10(4): 289–300, doi: 10.1007/BF02843829

Garrett C J R, Loucks H. 1976. Upwelling along the Yarmouth shore of Nova Scotia. Journal of the Fisheries Research Board of Canada, 33(1): 116–117, doi: 10.1139/f76-013

Ge Renfeng, Guo Jingsong, Yu Fei, et al. 2006. Classification of vertical temperature structure and thermocline analysis in the Yellow Sea and East China Sea shelf sea areas. Advances in Marine Science, 24(4): 424–435

Guan Bingxian. 1963. A preliminary study of the temperature variations and the characteristics of the circulation of the Cold Water Mass of the Yellow Sea. Oceanologia et Limnologia Sinica, 5(4): 255–284

Guo Binghuo, Xia Zongwan. 1986. A numerical model on the upwelling induced by tidal currents surrounding peninsulas. Haiyang Xuebao (in Chinese), 8(3): 272–282

He Chongben, Wang Yuanxiang, Lei Zongyou, et al. 1959. A preliminary study of the formation of Yellow Sea Cold Mass and its properties. Oceanologia et Limnologia Sinica, 2(1): 11–15

Hur H B, Jacobs G A, Teague W J. 1999. Monthly variations of water masses in the Yellow and East China Seas, November 6, 1998. Journal of Oceanography, 55(2): 171–184, doi: 10.1023/A:1007885828278

Jiang Beijie, Bao Xianwen, Wu Dexing, et al. 2007. Interannual variation of temperature and salinity of northern Huanghai Sea Cold Water Mass and its probable cause. Haiyang Xuebao (in Chinese), 29(4): 1–10

Li Ang, Yu Fei, Diao Xinyuan. 2015. Interannual salinity variability of the Northern Yellow Sea Cold Water Mass. Chinese Journal of Oceanology and Limnology, 33(3): 779–789, doi: 10.1007/s00343-015-4210-y

Lie H J. 1986. Summertime hydrographic features in the southeastern Hwanghae. Progress in Oceanography, 17(3–4): 229–242, doi: 10.1016/0079-6611(86)90046-7

Lie H J, Cho C H. 2016. Seasonal circulation patterns of the Yellow and East China Seas derived from satellite-tracked drifter trajectories and hydrographic observations. Progress in Oceanography, 146: 121–141, doi: 10.1016/j.pocean.2016.06.004

Liu Chuanyu, Wang Fan. 2009. Distributions and intra-seasonal evolutions of the sea surface thermal fronts in the Yellow Sea warm current origin area. Marine Sciences, 33(7): 87–93

Liu Guimei, Wang Hui, Sun Song, et al. 2003. Numerical study on the velocity structure around tidal fronts in the Yellow Sea. Advances in Atmospheric Sciences, 20(3): 453–460, doi: 10.1007/BF02690803

Lü Xingang, Qiao Fangli, Xia Changshui, et al. 2010. Upwelling and surface cold patches in the Yellow Sea in summer: Effects of tidal mixing on the vertical circulation. Continental Shelf Research, 30(6): 620–632, doi: 10.1016/j.csr.2009.09.002

Mao H L, Ren Yunwu, Wan K M. 1964. A preliminary investigation on the application of using *T-S* diagrams for a quantitative analysis of the watermasses in the shallow water area. Oceanologia et Limnologia Sinica, 6(1): 1–22

Mellor G L, Yamada T. 1982. Development of a turbulence closure model for geophysical fluid problems. Reviews of Geophysics, 20(4): 851–875, doi: 10.1029/RG020i004p00851

Naimie C E, Blain C A, Lynch D R. 2001. Seasonal mean circulation in the Yellow Sea—a model-generated climatology. Continental Shelf Research, 21(6–7): 667–695, doi: 10.1016/S0278-4343(00)00102-3

Oh K H, Lee S, Song K M, et al. 2013. The temporal and spatial variability of the Yellow Sea Cold Water Mass in the southeastern Yellow Sea, 2009–2011. Acta Oceanologica Sinica, 32(9): 1–10, doi: 10.1007/s13131-013-0346-9

Qiao Fangli, Ma Jian, Xia Changshui, et al. 2006. Influences of the surface wave-induced mixing and tidal mixing on the vertical temperature structure of the Yellow and East China Seas in summer. Progress in Natural Science, 16(7): 739–746, doi: 10.1080/10020070612330062

Ren Huijun, Zhan Jiemin. 2005. A numerical study on the seasonal variability of the Yellow Sea cold water mass and the related dynamics. Journal of Hydrodynamics, 20(S1): 887–896

Shu Yeqiang, Wang Dongxiao, Feng Ming, et al. 2018a. The contribution of local wind and ocean circulation to the interannual variability in coastal upwelling intensity in the northern South China Sea. Journal of Geophysical Research: Oceans, 123(9): 6766–6778, doi: 10.1029/2018JC014223

Shu Yeqiang, Wang Qiang, Zu Tingting. 2018b. Progress on shelf and slope circulation in the northern South China Sea. Science China Earth Sciences, 61(5): 560–571, doi: 10.1007/s11430-017-9152-y

Simpson J H, Hunter J R. 1974. Fronts in the Irish Sea. Nature, 250(5465): 404–406, doi: 10.1038/250404a0

Wan Zhenwen, Qiao Fangli, Yuan Yeli. 1998. Three-dimensional numerical modelling of tidal waves in the Bohai, Yellow and East China Seas. Oceanologia et Limnologia Sinica, 29(6): 611–616

Wang Dongxiao, Shu Yeqiang, Xue Huijie, et al. 2014. Relative contributions of local wind and topography to the coastal upwelling intensity in the northern South China Sea. Journal of Geophysical Research: Oceans, 119(4): 2550–2567, doi: 10.1002/2013JC009172

Wang Dongxiao, Zhuang Wei, Xie Shangping, et al. 2012. Coastal upwelling in summer 2000 in the northeastern South China Sea. Journal of Geophysical Research: Oceans, 117(C4): C04009, doi: 10.1029/2011JC007465

Weng Xuechuan, Zhang Yiken, Wang Congmin, et al. 1989. The variational characteristics of the Huanghai Sea (Yellow Sea) cold water mass. Journal of Ocean University of Qingdao, 19(S1): 119–131

Xia Zongwan, Guo Binghuo. 1983. Cold water and upwelling around the tips of Shandong Peninsula and Liaodong Peninsula. Journal of Oceanography of Huanghai & Bohai Seas (in Chinese), 1(1): 13–19

Xia Changshui, Qiao Fangli, Yang Yongzeng, et al. 2006. Three-dimensional structure of the summertime circulation in the Yellow Sea from a wave-tide-circulation coupled model. Journal of Geophysical Research: Oceans, 111(C11): C11S03

Xia Changshui, Qiao Fangli, Zhang Mengning, et al. 2004. Simulation of double cold cores of the 35°N section in the Yellow Sea with a

wave-tide-circulation coupled model. Chinese Journal of Oceanology and Limnology, 22(3): 292–298, doi: 10.1007/BF02842562

Xu Dongfeng, Yuan Yaochu, Liu Yuan. 2003. The baroclinic circulation structure of Yellow Sea Cold Water Mass. Science in China Series D: Earth Sciences, 46(2): 117–126, doi: 10.1360/03yd9011

Yanagi T, Takahashi S. 1993. Seasonal variation of circulations in the East China Sea and the Yellow Sea. Journal of Oceanography, 49(5): 503–520, doi: 10.1007/BF02237458

Yang H W, Cho Y K, Seo G H, et al. 2014. Interannual variation of the southern limit in the Yellow Sea Bottom Cold Water and its causes. Journal of Marine Systems, 139: 119–127, doi: 10.1016/j.jmarsys.2014.05.007

Yu Fei, Zhang Zhixin, Diao Xinyuan, et al. 2006. Analysis of evolution of the Huanghai Sea Cold Water Mass and its relationship with adjacent water masses. Haiyang Xuebao (in Chinese), 28(5): 26–34

Yuan Dongliang, Li Yao, Wang Bin, et al. 2017. Coastal circulation in the southwestern Yellow Sea in the summers of 2008 and 2009. Continental Shelf Research, 143: 101–117, doi: 10.1016/j.csr.2017.01.022

Zhang Yuankui, He Xianming. 1989. The annual variation and its forecasting of the intensity of cold water mass of the western-North Yellow Sea in spring. Journal of Ocean University of Qingdao, 19(S1): 275–282

Zhang Yuankui, He Xianming, Gao Yongfu. 1983. Preliminary analysis on the modified water masses in the North Yellow Sea and the Bohai Sea. Transactions of Oceanology and Limnology, (2): 19–26

Zhang Heng, Zhu Jianrong, Wu Hui. 2005. Numerical simulation of eight main tidal constituents in the East China Sea, Yellow Sea and Bohai Sea. Journal of East China Normal University (Natural Science), (3): 71–77

Zhao Baoren. 1986. The fronts of the Huanghai Cold Water Mass (HCWM) induced by tidal mixing. Chinese Journal of Oceanology and Limnology, 4(2): 159–170, doi: 10.1007/BF02850432

Zhao Baoren. 1987a. A preliminary study of continental shelf fronts in the western part of southern Huanghai Sea and circulation structure in the front region of the Huanghai cold water mass (HCWM). Oceanologia et Limnologia Sinica, 18(3): 217–227

Zhao Baoren. 1987b. The continental shelf fronts induced by tidal mixing in the Huanghai Sea. Journal of Oceanography of Huanghai & Bohai Sea (in Chinese), 5(2): 16–23

Zhou Chunyan, Dong Ping, Li Guangxue. 2015. A numerical study on the density driven circulation in the Yellow Sea Cold Water Mass. Journal of Ocean University of China, 14(3): 457–463, doi: 10.1007/s11802-015-2759-x

Zhu Junying, Shi Jie, Guo Xinyu, et al. 2018. Air-sea heat flux control on the Yellow Sea Cold Water Mass intensity and implications for its prediction. Continental Shelf Research, 152: 14–26, doi: 10.1016/j.csr.2017.10.006

Zou Emei, Guo Binghuo, Tang Yuxiang, et al. 2001. An analysis of summer hydrographic features and circulation in the southern Yellow Sea and the northern East China Sea. Oceanologia et Limnologia Sinica, 32(3): 340–348